Available online at www.sciencedirect.com
SCIENCE DIRECT®
Geochimica et Cosmochimica Acta 70 (2006) 1888–1903
Geochimica
www.elsevier.com/locate/gca

Computer simulation of electron transfer at hematite surfaces

Sebastien Kerisit *, Kevin M. Rosso

Chemical Sciences Division, Pacific Northwest National Laboratory, Richland, WA 99352, USA

Received 2 September 2005; accepted in revised form 27 December 2005

Abstract

Molecular dynamics simulations in combination with ab initio calculations were carried out to determine the rate of electron transfer at room temperature in bulk hematite (α-Fe_2O_3) and at two low-index surfaces, namely the (012) and (001) surfaces. The electron transfer reactions considered here involve the II/III valence interchange between nearest-neighbor iron atoms. Two electron transfer directions were investigated, namely the basal plane and *c* direction electron transfers. Electron transfer rates obtained in bulk hematite were in good agreement with ab initio electronic structure calculations thus validating the potential model. The surfaces were considered both in vacuum and in contact with an equilibrated aqueous solution. The reorganization energy is found to increase significantly at the first surface layer and this value is little affected by the presence of water. In addition, in the case of the (012) surface, the electronic coupling matrix element for the topmost basal plane transfer was calculated at the Hartree-Fock level and was found to be weak compared to the corresponding electron transfer in the bulk. Therefore, most surfaces show a decrease in the rate of electron transfer at the surface. However, where iron atoms involved in the electron transfer reaction are directly coordinated to water molecules, water lowers the free energy of activation to a great extent and provides a large driving force for electrons to diffuse toward the bulk thus opposing the intrinsic surface effect. The surfaces considered in this work show different electron transfer properties. Hematite has been shown to exhibit anisotropic conductivity and thus different surfaces will show different intra- and inter-layer rates depending on their orientation. Moreover, the calculations of electron transfers at the hydroxyl- and iron-terminated (001) surfaces revealed that surface termination has a significant effect on the electron transfer parameters in the vicinity of the surface. Finally, our findings indicate that undercoordinated terminal iron atoms could act as electron traps at the surface.

1. Introduction

Dissimilatory iron-reducing bacteria (DIRB) are capable of electron transfer to iron oxide minerals, such as hematite (α-Fe_2O_3), as part of their anaerobic respiration process. The addition of 'extra' electrons in the iron oxide lattice results in the reduction of iron(III) to iron(II) by the formation of small polarons (Rosso et al., 2003a). The larger iron(II) cations are more easily detached from the surface and hence the bacteria effectively promote mineral dissolution. This phenomenon is of great interest to the geochemical community due to its major role in the cycling of iron and has been the focus of many studies (Lovley, 1991; Lovley et al., 1996; Zachara et al., 1998; Newman and Kolter, 2000; Neal et al., 2003; Rosso et al., 2003b). However, the actual mechanisms of electron transfer are still unclear. One of the key questions is whether direct contact between the bacteria and the mineral surface is required for electron transfer to occur. Rosso et al. (2003b) carried out AFM experiments to probe the bioreduction of hematite surfaces by *Shewanella putrefaciens* CN32. This study showed that dissolution features, such as etching at growth centers and etch channels, arose from exposure to the bacteria but that these were clearly distinct from points of attachment. One possible explanation for this phenomenon is the presence of electron shuttle compounds as suggested by several research groups (Lovley et al., 1996; Newman and Kolter, 2000; Rosso et al., 2003b). Indeed, DIRB can produce quinone-related molecules that are thought to shuttle electrons to iron(III) oxides (Lovley et al., 1996; Newman and Kolter, 2000).

* Corresponding author. Fax: +1 509 376 3650.
E-mail address: sebastien.kerisit@pnl.gov (S. Kerisit).

0016-7037/$ - see front matter © 2006 Elsevier Inc. All rights reserved.
doi:10.1016/j.gca.2005.12.021

An alternative, or complementary, explanation is the transfer of electrons from the points of cell attachment to reactive sites through the hematite lattice. In order to evaluate the validity of this hypothesis, one needs to be able to compute the rate of electron transfer in the hematite lattice. To begin to address this, we must first acknowledge that polaron motion in crystal lattices can follow two mechanisms (Yamashita and Kurosawa, 1958; Holstein, 1959a,b): a band or tunneling process, which occurs at low temperature and an activated hopping process, which dominates at high temperature. There is evidence, in the literature, that conduction takes place via a hopping mechanism in hematite at room temperature (Goodenough, 1971; Benjelloun et al., 1984; Gharibi et al., 1990; Papaioannou et al., 2005), and hence can be treated within the framework of Marcus' theory (Marcus and Sutin, 1985). Moreover, the temperature above which the hopping mechanism dominates can be estimated from half the Debye temperature (Holstein, 1959b). Using published values of the longitudinal and shear wave velocities for natural hematite single crystals (Shapira, 1969) and Debye theory, the transition temperature is estimated to be about 200 K, thus providing further indication that polaron motion is in the hopping regime at room temperature.

In recent publications by Rosso et al. (2003a) and Iordanova et al. (2005), it was shown that electron transfer rates in bulk hematite can be determined from ab initio calculations using Marcus' theory. In addition, results obtained with this method reproduced the known anisotropy of the electron mobility between the directions perpendicular and parallel to the *c* axis (Nakau, 1960; Benjelloun et al., 1984). However, this approach cannot easily be extended to consider larger systems. Hence, we developed a new strategy which combines molecular dynamics simulations for the calculation of most of the electron transfer parameters in Marcus' theory, such as the reorganization energy and the free energy of electron transfer, with electronic structure calculations to compute the electronic coupling matrix element. Therefore, this method allows the investigation of electron transfer at a mineral surface to be computationally accessible while retaining an explicit treatment of the relevant electronic interactions. In a previous work (Kerisit and Rosso, 2005), this approach was successfully applied to the study of electron transfer in FeO, where the rates of electron transfer were in good agreement with ab initio calculations.

In this paper, we seek to evaluate how the kinetic and thermodynamic properties of electron transfer reactions at the mineral surface differ from those in the bulk. Furthermore, we aim to address the question: are the electrons free to diffuse away from the initial acceptor site at an appreciable rate? In doing so, we wish to determine whether charge transport through the mineral lattice plays an important role in the DIRB respiration process. We first test the validity of our method, to the study of electron transfer in hematite, by comparing the results obtained with two potential models with the rates reported previously for the transport of charges in hematite (Rosso et al., 2003a; Iordanova et al., 2005). Next, we investigate the kinetics of electron transfer at the (001) and (012) hematite surfaces. These surfaces are the most abundant hematite surfaces and their atomic structures and properties have been extensively studied both experimentally (Junta-Rosso and Hochella, 1996; Condon et al., 1998; Thevuthasan et al., 1999; Henderson, 2002, 2003; Trainor et al., 2004) and theoretically (Wasserman et al., 1997; Wang et al., 1998; Parker et al., 1999; Shaikhutdinov and Weiss, 1999; Jones et al., 2000; Cooke et al., 2004). In addition, these surfaces have been closely looked at in aqueous solution as well as in vacuum. For example, Henderson and coworkers (Henderson et al., 1998; Henderson, 2002) have investigated the interaction of water with the (012) surface with a range of experimental techniques while Rustad and coworkers used atomistic simulations (Wasserman et al., 1997, 1999; Rustad et al., 1999). Also, Thevuthasan et al. (1999) and Chambers and Yi (1999) have probed the structure of the (001) surface under ultrahigh vacuum conditions. Therefore, each surface will be considered in vacuum and in contact with water. In addition, in the case of the (001) surface, we investigated two possible surface terminations, namely the oxygen- and iron-terminated surfaces. Several studies have shown the metal termination to be the most stable surface (Chambers and Yi, 1999; Thevuthasan et al., 1999; Rohrbach et al., 2004). However, the coexistence of O- and Fe-terminated domains has also been observed (Shaikhutdinov and Weiss, 1999; Eggleston et al., 2003; Trainor et al., 2004) and predicted from electronic structure calculations (Wang et al., 1998; Trainor et al., 2004). However, we will first give a brief description of the theoretical methods used in this work.

2. Theoretical methods

2.1. Electron transfer model

The aim of this work is to determine the rate of electron transfer in the hematite lattice and at two of its low-index surfaces. To do so, an iron(III) is first replaced by an iron(II) thus effectively introducing an 'extra' electron in the mineral. We then consider the transfer of this electron to an adjacent iron(III). In a previous study (Rosso et al., 2003a), it was shown that it is appropriate to model an extra electron in the hematite lattice as localized in the form of a small polaron centered at an iron site. To calculate the rate of electron transfer, we need to compute the relevant electron transfer parameters, namely, the reorganization energy, the electronic coupling matrix element, the diabatic free energy of activation, and the free energy of reaction, to be used in Marcus' theory (Marcus and Sutin, 1985). The reorganization energy, λ, is the energy to distort the configuration of the reactants into that of the products, or vice versa, without changing the electronic distribution; the diabatic free energy of activation, $\Delta G^{*'}$, is the energy required to thermally excite the system to the transition state configuration; the free

energy of reaction, ΔG^0, is the change in free energy upon electron transfer; and the electronic coupling matrix element, V_{AB}, is the amount of electronic interaction between the reactant and product states at the transition state. These parameters are explained graphically in Fig. 1. In the past, two different approaches have been used in this group to generate a free energy diagram such as the one in Fig. 1 and calculate the electron transfer parameters. The first method consists in extracting small clusters from a periodic electronic structure calculation of the 'defective' lattice and performing single-point energy calculations at the unrestricted Hartree-Fock (UHF) level of a few relevant points on the curves (e.g., minima and crossing point) (Rosso et al., 2003a; Iordanova et al., 2005). When we refer to the 'defective' lattice, we refer to the lattice bearing an extra electron, i.e., an iron(II) atom. An additional calculation is required to compute the electronic coupling matrix element at the crossing point configuration (labeled 'C' in Fig. 1). In this approach, the atomic interactions are treated at a high level of theory but the method is limited to systems that can be modeled with relatively small clusters. It is thus the method of choice for bulk systems for example but can be problematic for heterogeneous systems. In the second method, the two free energy curves are computed from classical molecular dynamics simulations of a supercell using the umbrella sampling technique. This method enables us to investigate larger systems and thus to consider, for example, electron transfer reactions at a mineral surface. In addition, this approach includes an explicit treatment of the temperature. Although the electronic structure of the system is not computed in this method, a UHF calculation is performed on a small cluster representing the atoms directly involved in the electron transfer process to calculate the electronic coupling. In a previous work (Kerisit and Rosso, 2005), we showed that the configuration used for the electronic coupling calculation can be obtained from an energy minimization of the system with a potential model, thus avoiding the need to carry out a computationally expensive ab initio energy minimization. In summary, this method retains an explicit representation of the relevant electronic interactions while exploiting the fact that a classical approach is sufficient to reliably obtain the relative energies of the different states of interest.

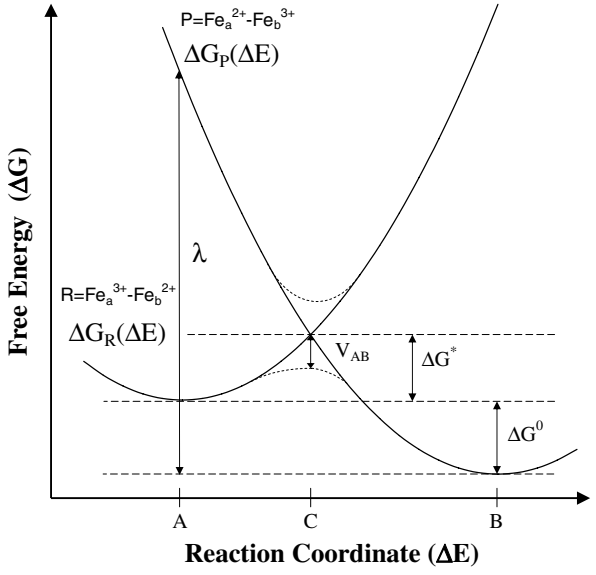

Fig. 1. Free energy diagram of an electron transfer reaction.

In what follows, we describe in more detail the two approaches mentioned above. However, we will limit ourselves to the essential concepts; for a complete discussion of these methods, see Rosso et al. (2003a), Iordanova et al. (2005) and Kerisit and Rosso (2005). In the molecular dynamics approach, the reaction coordinate (also referred to as the energy gap) is defined as the energy difference between the normal and reversed charge states for a particular configuration of the system. The free energy curves are calculated from the probability of finding the system in a state for which $\Delta E = X$ versus the probability of being in a state for which $\Delta E = \langle \Delta E \rangle$:

$$\Delta G(X) = -RT \ln \left[\frac{P(X)}{P(\langle \Delta E \rangle)} \right], \quad (1)$$

where $\langle \Delta E \rangle$ is the ensemble average of the energy gap. In theory, each free energy curve could be obtained from a single molecular dynamics simulation. The diabatic activation free energy would be the value of ΔG for $\Delta E = 0$. However, as it is often the case, the activation free energy is too high for the region of phase space in the vicinity $\Delta E = 0$ to be significantly sampled with a single molecular dynamics calculation. To overcome this problem, we employed the umbrella sampling technique as first introduced, for an electron transfer reaction, in seminal papers by Hwang and Warshel (1987), Kuharski et al. (1988), and King and Warshel (1990). In this method, the charge and short-range parameters of the electron donor are gradually changed into those of the electron acceptor and vice versa. The new potential of the system is calculated from a linear combination of the reactant and product state potentials (V_A and V_B, respectively):

$$V_\theta = (1 - \theta) V_A + \theta V_B, \quad (2)$$

where θ is varied from 0 to 1 in a series of discrete values and a simulation is carried out for each value.

This biases the system to generate configurations that have values of ΔE significantly different from $\langle \Delta E \rangle$. Therefore, a thorough sampling of the phase space along the reaction coordinate is achieved. The bias thus introduced is removed, once the simulation has been run, by adjusting the free energy as follows [see Kuharski et al., 1988 for detail of the derivation of Eq. (3)]:

$$\Delta G(X) = -RT \ln \left[\frac{P(X)_\theta}{P(\langle \Delta E \rangle)} \right] - \theta X + C, \quad (3)$$

where C is a normalization constant and $P(X)_\theta$ is the probability of finding the system at $\Delta E = X$ when its potential is V_θ. Finally, the Frank–Condon principle states that the electronic transfer is instantaneous relative to the nuclei

motion and hence the system polarizability needs to be calculated for both the normal and reversed charge states. The first modeling study of electron transfer with a polarizable potential model is by Rustad et al. (2004), who used an extended Lagrangian technique to treat the polarizability of oxygen ions. As our model accounts for the polarizability of anions by means of a shell model, the position of the shells must be relaxed for each normal and reversed charge state configuration used in Eq. (3). The energy minimization of the shells is carried out using the steepest descent method as implemented in the computer code DL_POLY (Smith and Forester, 1996).

In the ab initio cluster approach, a periodic electronic structure calculation is first performed to determine the structure of the defective lattice. Then, small clusters are excised from the periodic calculation and the overall charge is neutralized by adding protons along the cleaved bonds to preserve the symmetry of the structure. The oxygen valence requirements are also taken into account in the protonation scheme. The reorganization energy is divided into two components, namely, the internal and external parts. The internal part can be calculated from the so-called direct method (Rosso et al., 2003a; Rosso and Dupuis, 2004) or the four-point (Nelsen et al., 1987) method using the excised clusters. The external part is the energy to polarize the remainder of the system upon electron transfer and is calculated using a dielectric continuum model. Finally, the electronic coupling matrix element, V_{AB}, is computed following the approach developed for use with electronic structure calculations by Farazdel et al. (1990). As already mentioned, V_{AB} accounts for the electronic interaction between the normal and reversed charge states at the crossing point configuration. If the free energy curves are assumed to be parabolic, as is often the case, the reaction coordinate can be approximated by

$$q(\xi) = (1-\xi)q_A + \xi q_B, \tag{4}$$

where q_A and q_B are the nuclear coordinates of the reactant and product states, respectively. By varying ξ, the nuclear coordinates of any point along the reaction coordinate can be determined. V_{AB} is defined as half the energy difference between the upper and lower adiabatic surfaces at the crossing point configuration (Farazdel et al., 1990):

$$V_{AB} = \frac{|H_{AB} - S_{AB}(H_{AA}+H_{BB})/2|}{1-S_{AB}^2}, \tag{5}$$

where H_{AB} is the interaction energy ($H_{AB} = \langle\psi_A|H|\psi_B\rangle$), S_{AB} is the overlap between the reactant and product states ($S_{AB} = \langle\psi_A|\psi_B\rangle$), and H is the total electronic Hamiltonian.

The rate of electron transfer can take place in two different regimes, namely, adiabatic and nonadiabatic, depending mainly on the strength of the electronic coupling. The adiabatic criterion is used to determine whether an electron transfer is adiabatic or nonadiabatic and is calculated as follows:

$$\kappa = 2P_{12}^0/(1+P_{12}^0), \tag{6}$$

where

$$P_{12}^0 = 1 - \exp\left(-\left(V_{AB}^2/h\upsilon_n\right)\sqrt{\pi^3/\lambda k_B T}\right), \tag{7}$$

where h is Planck's constant, υ_n is a typical frequency for nuclear motion, k_B is Boltzmann's constant and T is the temperature (this form assumes that the electron transfer reaction is symmetric). When the coupling is strong the transmission coefficient equals one and the electron transfer is adiabatic and the rate expression is as follows:

$$k_{et} = n\upsilon_n \exp(-\Delta G^*/k_B T), \tag{8}$$

where

$$\Delta G^* = \frac{(\lambda+\Delta G^0)^2}{4\lambda} - V_{AB} \tag{9}$$

and n is the number of sites available for electron transfer. However, if the electronic coupling is weak, the electron transfer is nonadiabatic and the rate constant takes the following expression (Marcus and Sutin, 1985):

$$k_{et} = \frac{2\pi}{\hbar}|V_{AB}|^2 \frac{1}{\sqrt{4\pi\lambda k_B T}} \exp\left[-\frac{(\Delta G^0+\lambda)^2}{4\lambda k_B T}\right]. \tag{10}$$

2.2. Molecular dynamics simulations

The molecular dynamics simulations presented in this work were performed using the computer code DL_POLY (Smith and Forester, 1996). These calculations are based on the Born model of solids (Born and Huang, 1954), whereby atoms are represented by point-charge particles which interact via long-range Coulombic forces and short-range forces. The short-range forces are described by parameterized functions and account for the repulsion between electron-charge clouds, the van der Waals attraction forces, and, where appropriate, covalent effects by means of an angle-dependent term. Another important feature of our model is that the polarizability of anions is represented by a shell model. In this model, first introduced by Dick and Overhauser (1958), a polarizable ion is composed of two particles, a core and a shell, which share the ion's charge and are linked by an harmonic spring. In a previous paper (Kerisit and Rosso, 2005), we showed that a shell model is essential to reproduce the electron transfer parameters obtained from ab initio calculations. Simulations of the bulk hematite lattice were performed in the NPT ensemble (constant number of particles, constant pressure, and constant temperature), whereas the surface simulations were carried out in the NVT ensemble (constant number of particles, constant volume, and constant temperature). All calculations were run at 300 K and zero pressure. The temperature and pressure were kept constant by use of the Nosé-Hoover thermostat (Hoover, 1985) and the Hoover barostat (Hoover, 1985; Melchionna et al., 1993), respectively. The electrostatic forces were calculated by means

of the Ewald summation method (Ewald, 1921). An 8 Å cutoff was used for the short-range interactions and the real part of the Ewald sum. The Verlet leapfrog algorithm was used to integrate the equations of motion with a time step of 0.2 fs. The shells were given a mass of 0.2 a.u. and their motion treated as that of the cores following the adiabatic shell model first introduced by Mitchell and Fincham (1993). The electron transfer calculations in bulk hematite were carried out with two sets of potential parameters. The first set is that of Lewis and Catlow (1985), including the modified Fe(II)–oxygen Buckingham potential derived in a previous paper (Kerisit and Rosso, 2005). These potential parameters have been used to model iron oxide minerals on many occasions (Davies et al., 1989; Parker et al., 1999; Jones et al., 2000; Cooke et al., 2004). The second set was developed by Bush et al. (1994a,b) with the iron(III)–oxygen potential later introduced by Woodley et al. (1999). This model has also been applied to the simulation of iron oxides many times (Berry et al., 1998, 1999; Ayub et al., 2001; Moore et al., 2002). The intra- and intermolecular interactions of water were described by the shell model of de Leeuw and Parker (1998) with the modified hydrogen bond potential of Kerisit and Parker (2004). The potential parameters for the hydroxyl ion were derived by Baram and Parker (1996). The iron-hydroxyl oxygen potentials were obtained from a simple scaling of the iron–lattice oxygen potentials to the hydroxyl oxygen charge. The interactions between iron(II) and (III) and water were based on the iron–water potentials of Curtiss et al. (1987). These potential parameters were modified to be compatible with the water model used in this work. The parameters were refitted to first match the binding energies and iron–water distances of the iron(II) and iron(III) hexaaquo complexes in the gas-phase. In addition, molecular dynamics simulations of a single iron(II) or iron(III) ion in a cubic box containing 255 water molecules were carried out over 700 ps to evaluate whether the potential parameters were able to reproduce the solvation energies, the coordination numbers, and the iron–water first shell distances (see EA-1 in Supplementary material). Tables EA3 and EA4 in Supplementary material show that, although the iron–water distances, the gas-phase binding energies, and the solvation energies are slightly underestimated, the differences between the values for the two oxidation states are in very good agreement with experimental data and electronic structure calculations.

2.3. Ab initio calculations

Ab initio calculations were performed to compute V_{AB} for the basal plane transfer in bulk hematite and at the dry and hydrated (012) surface. First, clusters of pairs of iron octahedra were excised from energy minimizations of the systems of interest with a potential model. The iron atoms were ferromagnetically coupled according to the magnetic structure of hematite in the basal plane. Note that the V_{AB} value for the c direction electron transfer was taken from the cluster calculations of Iordanova et al. (2005) where the iron atoms were antiferromagnetically coupled to represent the known magnetic structure of hematite. Then, the clusters were charge neutralized using a protonation scheme described elsewhere (Rosso et al., 2003a; Iordanova et al., 2005) for use in ab initio cluster calculations. The effect of protons on the value of the electronic coupling is thought not to be significant as a previous study (Rosso et al., 2003a) has shown that the overlap between the reactant and product states is due to the iron 3d orbitals and a superexchange contribution through the bridging oxygen atoms. The calculations of the electronic coupling matrix elements were carried out with NWCHEM (Straatsma et al., 2004) at the spin unrestricted HF level with the Ahlrichs valence triple-zeta basis set for iron (Schafer et al., 1994), which was augmented with three diffuse functions (function/exponent = s/0.01257, p/0.04184, d/0.11330) (Clark et al., 1983) and the 6-311G basis set for the oxygen and hydrogen atoms (Krishnan et al., 1980). The effect of electron correlation on the values of V_{AB} was not included as these calculations were based on the UHF wave functions of the reactant and product states.

3. Results and discussion

3.1. Bulk hematite

To evaluate the accuracy of the molecular dynamics approach, we first investigated the rate of electron transfer in the hematite bulk lattice and compared the results thus obtained to those published by Iordanova et al. (2005). In addition, as mentioned in Section 2, the calculations were performed with two different potential models. As done previously (Kerisit and Rosso, 2005), we considered four values of θ (i.e., 0.000, 0.167, 0.333, and 0.500) and a 1 ns MD simulation was carried out for each value. For more detail on why these four values are sufficient see Kerisit and Rosso (2005) and references therein. We considered the same two nearest-neighbor electron transfers as in Iordanova et al. (2005), namely the basal plane and c direction transfers. The latter involves electron transfer between two face-sharing FeO_6 octahedra, whereas the former occurs between two edge-sharing octahedra. At this point it should be noted that in nature, all the iron atoms in the hematite lattice are in a high-spin d^5 configuration with their spins ferromagnetically coupled in the basal plane and antiferromagnetically in the c direction. In a classical view, this implies that the transfer of an 'extra' electron in the c direction is spin forbidden because a high-spin d^5 iron(III) atom cannot accept the minority spin electron from the adjacent high-spin d^6 iron(II) atom along the c direction. For this reason, one might anticipate conductivity in hematite to be anisotropic (Goodenough, 1971). Indeed, experiments have shown that electron transfer in this direction is three to four orders of magnitude lower than in the basal plane (Nakau, 1960; Benjelloun et al., 1984). However, Iordanova et al. (2005) found that this

difference was mainly due to a weak electronic coupling, as shown in Table 1, as opposed to being due to apparent spin restrictions. In fact, the 'minority-spin' description is not strictly valid since electrons are fermions and electronic wave functions are antisymmetric with respect to the interchange of electrons (Iordanova et al., 2005).

The free energy curves for each potential model were generated for the two directions and the calculated electron transfer parameters and rate constants are summarized in Table 1, together with the corresponding values reported in Iordanova et al. (2005). As an example, the free energy curves obtained from the basal transfer with the Lewis and Catlow model are shown in Fig. 2. The free energy curves are parabolic. This is an important point as it is an assumption of Marcus' theory. The two potential models bracket the ab initio value of the reorganization energy, with the Lewis and Catlow model yielding the higher value and the Bush et al. model the lower one. The three models predict a small difference in reorganization energy between the two directions; however, the relative difference, with respect to the basal plane transfer, predicted by the Bush et al. model (20%) is significantly larger than that obtained with the Lewis and Catlow model (7%) and by the electronic structure calculations (3.5%). It is important to note that the two approaches differ slightly in that the ab initio method is performed at 0 K whereas the MD calculations are carried out at 300 K. To investigate the effect temperature on the magnitude of the reorganization energy, we carried out reorganization energy calculations at 0 K with the Lewis and Catlow model using the direct method. The value at 0 K was calculated to be 1.70 eV (compared to 1.75 eV at 300 K) and thus, as seen previously in the case of FeO, the effect of temperature on the reorganization energy appears to be small.

Table 1
Electron transfer parameters and rates of electron transfer in bulk hematite calculated from the molecular dynamics method and the ab initio cluster approach

Model	Transfer	λ (eV)	V_{AB} (eV)	κ	i	ΔG^* (eV)	k (s^{-1})
Bush et al.	Basal	0.89	0.187	1.00	3	0.04	1.4E+13
Lewis et al.	Basal	1.75	0.184	1.00	3	0.25	3.2E+09
Ab initio	Basal	*1.42*	*0.190*	*1.00*	*3*	*0.19*	*3.4E+10*
Bush et al.	*c* direction	1.07	0.028	0.45	1	0.24	1.8E+09
Lewis et al.	*c* direction	1.88	*0.028*	0.37	1	0.44	6.5E+05
Ab initio	*c* direction	*1.47*	*0.028*	*0.40*	*1*	*0.34*	*3.3E+07*

Numbers in italics were taken from Iordanova et al. (2005).

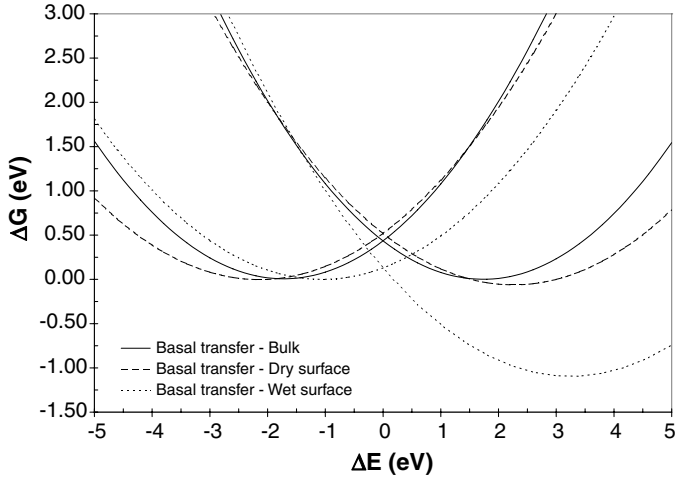

Fig. 2. Examples of free energy curves obtained from the simulations of electron transfer in bulk hematite and at the dry and hydrated (012) surface.

We also evaluated whether clusters excised from energy minimizations of the defective hematite lattice with the two potential models could be used as input to the calculation of the electronic coupling matrix element. We limited ourselves to the basal plane transfer as the calculation of the electronic coupling in the *c* direction requires complex and computationally expensive ab initio methods (Iordanova et al., 2005) that are beyond the scope of this paper. Table 1 shows that the electronic coupling in the basal plane is relatively independent of the model used to generate the crossing point configuration. A similar conclusion was drawn, in a previous paper (Kerisit and Rosso, 2005), from the calculation of the electronic coupling in FeO. This clearly indicates that, where nuclear coordinates from ab initio calculations are not available (e.g., surface electron transfer), we can use with confidence the structures obtained from classical simulations as input for the V_{AB} calculations.

The transmission coefficients are all of the order of one and hence the adiabatic rate expression Eq. (8) was used to calculate each rate constant. In Eq. (8), we use the same value of υ_n as was used by Iordanova et al. (2005), i.e., $1.85 \times 10^{13}\ s^{-1}$, which is the highest infra-red active longitudinal optic mode phonon. This value will be used throughout this paper. The rates obtained from the Lewis and Catlow model are in closer agreement with the ab initio calculations than those obtained with the Bush et al. model. Nonetheless, the two models correctly predicted a difference in rates, between the two directions, of three to four orders of magnitude in accord with experimental observations (Nakau, 1960; Benjelloun et al., 1984). As the Lewis and Catlow model performed best out of the two models, when compared to the electronic structure calculations, we decided to only consider this model in the remainder of this study, which is concerned with the electron transfer at the two principal hematite surfaces.

3.2. (012) Hematite surface

The (012) surface is terminated by a nonpolar plane containing both oxygen and iron atoms. The topmost iron atoms are coordinated to five oxygen atoms (as opposed to six in the bulk): four in the surface plane and one below. The surface is not perfectly flat as the surface octahedra are

tilted with respect to the surface normal, as shown in Fig. 3. Our model (012) hematite slab consisted of 192 Fe_2O_3 units for a total of 1536 particles including the shells. The surface area was 20.29×16.01 Å^2 and the slab was two unit cells thick (i.e., about 27 Å). We performed a series of calculations to determine the rate of electron transfer in the near-surface region when the surface is in vacuum. We considered all the nonequivalent electron transfers in one half of the hematite slab, i.e., in the first four layers. Due to the orientation of the surface, the nominally basal plane transfer can either occur within a surface layer or between two surface layers, as indicated by the atoms labeled 'B' and 'C' in Fig. 3. These electron transfers will be referred to as the intra- and inter-layer basal plane transfers, respectively. The *c* direction transfer, however, can only occur between two iron atoms of the same surface layer (atoms labeled 'A' in Fig. 3). Therefore, three different electron transfers can occur at the (012) surface.

We first carried out a 300 ps MD simulation of the model slab to allow it to come to mechanical equilibrium. Then, the final configuration from this run was used as the starting configuration for each value of θ in the umbrella sampling calculations. The simulation time was shortened to 300 ps in all the surface calculations reported in this paper. This was necessary as these simulations are computationally more expensive than the bulk calculations, especially when the surface is in contact with a slab of water. However, we did perform a test simulation of the intra-layer basal transfer in the first surface layer whereby the simulation time was increased to 1 ns for each value of θ, to investigate the effect of simulation time on the electron transfer parameters. The electron transfer parameters, namely the reorganization energy, the diabatic free energy of activation, and the free energy of reaction did not change significantly. The reorganization energy decreased from 2.20 to 2.14 eV, the free energy increased from −0.07 to −0.03 eV, and the diabatic activation free energy stayed constant at 0.52 eV. These results suggest that the simulation time can be reduced to 300 ps without any significant loss of accuracy.

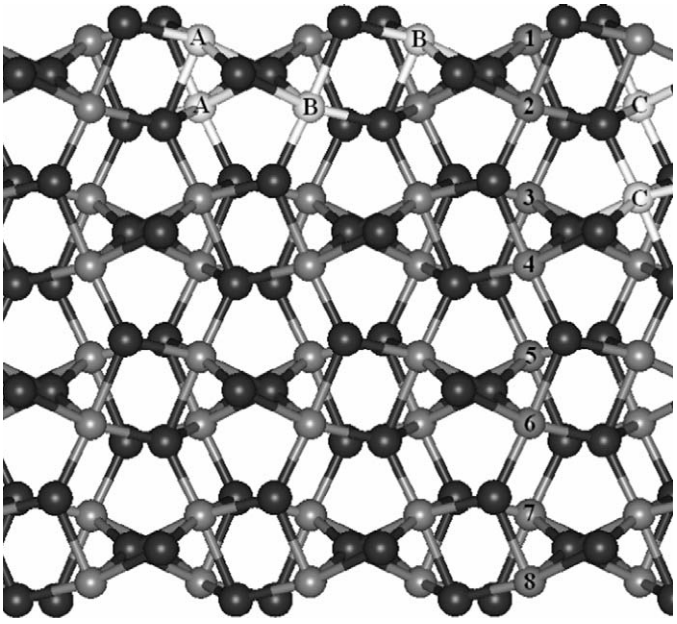

Fig. 3. Side view of the (012) hematite surface showing the three possible electron transfers, namely *c* direction (A), basal intra-layer (B), and basal inter-layer (C) transfers. Also shown are the first eight nonequivalent iron sites.

Table 2
Electron transfer parameters for electron transfer at the (012) surface both in vacuum and in contact with an aqueous solution

Layer(s)	Transfer	λ (eV)	V_{AB} (eV)	ΔG^0 (eV)	κ	i	ΔG^* (eV)	k (s^{-1})
In vacuum								
1	Basal-intra	2.20	0.017	−0.07	0.16	2	0.50	1.2E+05
1	*c* direction	2.17	0.028	0.01	0.35	1	0.52	3.1E+04
1–2	Basal-inter	1.81	0.184	0.33	1.00	1	0.45	5.7E+05
2	Basal-intra	1.72	0.184	−0.15	1.00	2	0.17	4.6E+10
2	*c* direction	1.91	0.028	−0.19	0.37	1	0.36	1.5E+07
2–3	Basal-inter	1.72	0.184	−0.02	1.00	1	0.24	1.9E+09
3	Basal-intra	1.70	0.184	0.06	1.00	2	0.27	9.2E+08
3	*c* direction	1.92	0.028	0.00	0.37	1	0.46	4.2E+05
3–4	Basal-inter	1.74	0.184	−0.02	1.00	1	0.24	1.6E+09
4	Basal-intra	1.76	0.184	−0.02	1.00	2	0.25	2.8E+09
4	*c* direction	1.86	0.028	−0.01	0.37	1	0.43	1.1E+06
4–5	Basal-inter	1.73	0.184	0.00	1.00	1	0.25	1.2E+09
In solution								
1	Basal-intra	2.15	0.031	−1.09	0.41	2	0.10	7.7E+11
1	*c* direction	2.17	0.028	−1.12	0.35	1	0.10	4.0E+11
1–2	Basal-inter	1.75	0.184	0.15	1.00	1	0.33	4.5E+07
2	Basal-intra	1.77	0.184	−0.08	1.00	2	0.22	8.4E+09
2	*c* direction	1.92	0.028	−0.07	0.37	1	0.42	1.8E+06
2–3	Basal-inter	1.70	0.184	0.06	1.00	1	0.27	5.0E+08
3	Basal-intra	1.74	0.184	0.02	1.00	2	0.26	1.6E+09
3	*c* direction	1.86	0.028	0.01	0.37	1	0.44	7.5E+05
3–4	Basal-inter	1.71	0.184	0.02	1.00	1	0.25	1.1E+09
4	Basal-intra	1.72	0.184	0.02	1.00	2	0.26	1.7E+09
4	*c* direction	1.90	0.028	−0.03	0.37	1	0.44	9.1E+05
4–5	Basal-inter	1.75	0.184	−0.02	1.00	1	0.24	1.5E+09

We performed a total of 12 electron transfer calculations at this surface (three directions in four layers). As an example, the free energy curves obtained from the simulation of the basal transfer in the first layer are shown in Fig. 2. The free energy curves for this transfer are parabolic and thus suggest that Marcus' parabolic assumption is also valid for electron transfers occurring at the surface. Table 2 summarizes the electron transfer parameters as a function of depth for the three directions considered. We shall now discuss each electron transfer parameter in turn. The reorganization energy increases drastically for those electron transfers that involve a terminal iron (25 and 15% for the basal plane and *c* direction transfers, respectively); however, it does not significantly differ from the bulk value for all the other electron transfers. To understand the cause of the change in reorganization energy at the surface, we computed the iron–oxygen radial distribution function (RDF) at several depths in the surface and also in the bulk, as shown in Fig. 4. A RDF of the iron(II)–oxygen distances shows that replacing an iron(III) by and iron(II) in bulk hematite causes a large splitting of the first peak, with a distance of

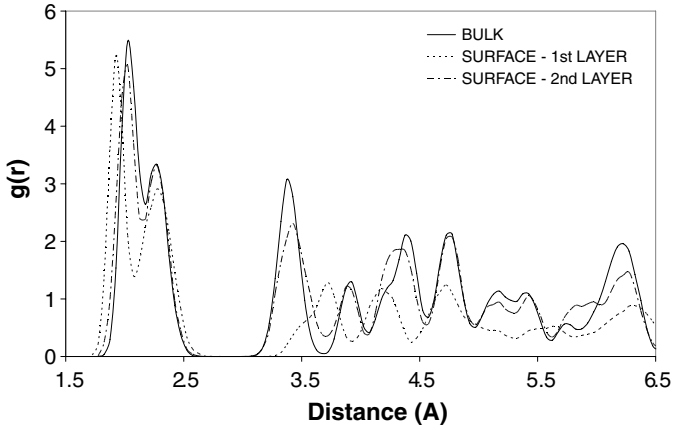

Fig. 4. Iron(II)–oxygen radial distribution functions in bulk hematite and at the first and second layers down the (012) surface. The first coordination shell of the surface—1st layer RDF was scaled by 6/5 for comparison purposes.

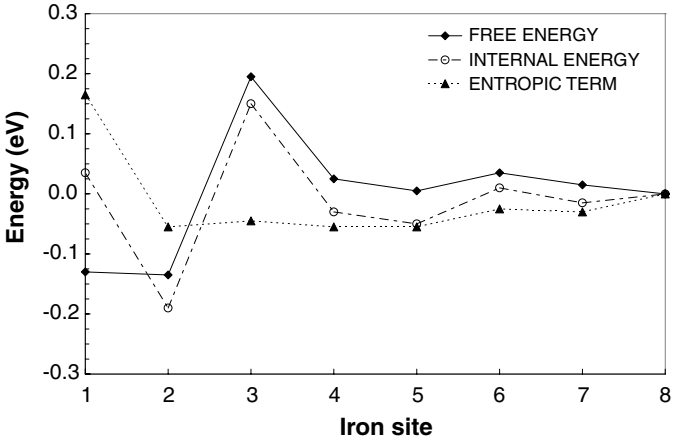

Fig. 5. Free energy, internal energy, and entropic term profiles of a small polaron at the (012) surface. The lines are provided as a guide to the eyes.

about 0.25 Å between the two maxima. This means that the reduced iron atoms form three long and three short bonds with oxygen atoms in their first coordination shell. It should be noted that the Fe(III)O_6 octahedra are also split but not to the same extent (only about 0.11 Å—data not shown). At the surface the splitting is increased to 0.35 Å due to the first part of the peak being shifted toward smaller distances. The minimum between the two peaks is also shifted to the left. As the terminal irons are only fivefold coordinated, we scaled the first peak by 6/5 in Fig. 4 for comparison purposes. An integration of the area underneath the first peak yields the average coordination, $n(r)$. This reveals that the terminal iron atoms have one less short bond than in the bulk (2.5 compared to 3.5) and thus one more long bond. Hence, the terminal Fe(II)O_6 octahedra are not only incomplete but also differ from those in the bulk in terms of bond length and number of bonds of each length. This deviation from the ideal geometry of the FeO_6 octahedron results in an increase of the reorganization energy. At all other positions the iron(II)–oxygen RDF resembles much more that of the bulk (see Fig. 4 for an example), which explains why a rapid convergence of the reorganization energy to its bulk value is observed.

Table 2 also shows the free energy of each electron transfer as a function of depth in vacuum. The intra-layer basal plane and c direction transfers take place between the same pair of iron atoms and thus, although the two electron transfers have different activation free energies, they should show identical free energies of reaction. The difference in free energy between these two electron transfers gives an indication of the precision of the method, which turns out to be less than 0.08 eV. From this table, we can generate the free energy profile of a small polaron as a function of depth. In addition, we can compute, from the umbrella sampling calculations where $\theta = 0$, the average internal energy of the system when the polaron is at each iron site. By subtracting the two curves we can deduce an approximate entropy change, as shown in Fig. 5, assuming that the internal energy is a good approximation to the enthalpy. Fig. 5 shows a maximum in free energy at the third site. This maximum is due to a large increase in internal energy when the electron is localized at this site. We generated the same internal energy curve from energy minimizations of the hematite slab for each position of the polaron and obtained an almost identical plot. This implies that the increase in internal energy is not due to the dynamical properties of the mineral slab but rather to the atomic relaxation in the near-surface region. Fig. 5 also shows that there is a small overall driving force (0.13 eV) for the polaron to diffuse to the surface, although the third iron site represents a barrier. From sites 4 to 8, the free energy difference is within the accuracy of the method and thus it is believed to be converged to its bulk value. Another interesting point is that the entropic term is small and constant for each site except for site 1. At this site, the internal energy increases and so does the entropic term, which suggests that the change in internal energy caused by the incomplete octahedra is, within the accuracy of the method, exactly compensated by the change in entropy, which is itself most likely due to the 'extra room' available at the topmost surface layer. As a consequence, there is no driving force for the electron to go from a terminal iron atom to an iron atom directly below. However, Table 2 also shows that the adiabatic activation free energy for electron transfer between these two atoms is higher than in the bulk. The activation free energy of the first interlayer basal transfer to site 3 is also high whereas it is slightly lower than in the bulk for the intra-layer basal transfer to site 4. The remaining electron transfers show activation free energies similar to those in the bulk.

We then investigated the effect of water on the rate of electron transfer at the surface. The hematite slab was put in contact with a slab of water containing 340 water molecules. The water slab had a thickness of about 25 Å. We only considered molecular water in contact with this surface as it was shown in a previous study (Kerisit

et al., 2005) to be the most stable adsorption mode of water on this surface when using a very a similar potential model. However, experimental work by Henderson and coworkers (Henderson et al., 1998; Henderson, 2002) and atomistic simulations by Rustad and coworkers (Wasserman et al., 1997, 1999; Rustad et al., 1999) showed strong evidence for dissociation of water at the surface. Therefore, we envisage to extend this work, in future studies, to the investigation of the effect of water dissociation at the (012) surface on the rate of electron transfer. A 300 ps MD simulation was carried out to let the system reach mechanical equilibrium. The same 12 electron transfers were considered and Table 2 shows the electron transfer parameters thus obtained as a function of depth. Again, as an example, the free energy curves obtained from the simulation of the basal transfer in the first layer are shown in Fig. 2. This figure suggests that the free energy curves are parabolic even when the surface is in contact with an aqueous solution. The somewhat surprising result is that water has little effect on the reorganization energy. However, water has a significant impact on the free energy of reaction. There is now a large driving force (about 1.1 eV) for the polaron to diffuse from site 1 to site 2. To evaluate whether this large change is due to the water molecules directly in contact with surface iron atoms or to the presence of the entire water slab, we carried out MD simulations of the intra-layer basal transfer in the first surface layer with a single monolayer of water adsorbed on the surface. A water molecule was adsorbed above each surface oxygen and iron atom for a total of 48 water molecules on each face of the slab. Again, a 300 ps MD simulation was performed to bring the system to mechanical equilibrium. The results were almost identical to the solution case. The reorganization energy was found to be 2.13 eV, the adiabatic activation free energy 0.11 eV, and the free energy of reaction −1.06 eV. This calculation suggests that the large change in free energy is mostly due to those water molecules in direct contact with the iron atoms involved in the electron transfer. Therefore, although moving the polaron from site 1 to site 2 increases the internal energy of the mineral slab due to a decrease in the number of iron(III)–lattice oxygen interactions, the large difference in binding energies with water between iron(II) and iron(III) more than compensates for this. In addition, we can see from Table 2 that the adiabatic activation free energy is considerably reduced from about 0.50 to 0.10 eV for both electron transfers in the first layer. Finally, water helps to stabilize site 3 and thus the magnitude of the activation free energy for electron transfers from and to that site is reduced. In conclusion, the results shown in Table 2 suggest that the influence of water is only significant in the first two surface layers and is most striking where there is direct contact with the iron atoms participating in the electron transfer reaction.

We also performed energy minimizations of the dry and hydrated surfaces (albeit with only one monolayer adsorbed), from which we excised iron dimer clusters to compute the electronic coupling matrix element. We assumed that V_{AB} would only differ from the bulk value for the electron transfers involving terminal iron atoms. In addition, as explained earlier, the calculation of V_{AB} for the c direction transfer is beyond the scope of this paper. Hence, we computed V_{AB} for the intra-layer basal plane transfer in the first layer in both dry and wet conditions. In both cases, we found V_{AB} to be significantly smaller than for the corresponding bulk electron transfers. This can be explained by the large deformation of the surface octahedra already mentioned. As was found for the reorganization energy, water has a limited effect on the value of V_{AB}.

Finally, we calculated the rate of each electron transfer for the vacuum and solution cases, as shown in Table 2. In vacuum conditions, the basal plane transfer between sites 1 and 2 is four orders of magnitude slower than in the bulk, mainly due to a large reduction of the electronic coupling but also in part due to the increase in activation and reorganization energies. The c direction transfer between these same two sites is only reduced by about one order of magnitude, however we would expect V_{AB} to actually be smaller and thus the difference in rate could be greater. The first inter-layer basal transfer is also four orders of magnitude slower than in the bulk. Although the electronic coupling is large, and again the actual value could be smaller, the very high diabatic activation energy (0.63 eV) results in a significant reduction of the rate. In the second layer, we see a slight acceleration of the rate and deeper in the slab, from layer 3, the rate of electron transfer is comparable to that in the bulk. When the slab is put in contact with an aqueous solution, the rate of electron transfer in the first layer becomes two orders of magnitude faster than in the bulk. The intrinsic effect of the surface, which tends to slow down electron diffusion, is counter-balanced by a large driving force to maximize the number of Fe(III) at the surface. It is interesting to note that the anisotropy seen in the bulk disappears in the first layer. The first inter-layer basal transfer is still slower than in the bulk but is two orders of magnitude faster that in the vacuum case. Again, the rates in layers 3 and 4 are similar to those observed in the bulk.

In summary, the first two surface layers show very different electron transfer parameters than in the bulk. The inherent effect of the surface is to slow down the electron diffusion due to an increase in reorganization energy and a decrease in electronic coupling. However, the presence of water opposes that effect by reducing the activation free energy and greatly stabilizing iron(III) at the surface, which causes the rate for electron transfer away from the surface to increase significantly in the first layer. Nonetheless, water does not eliminate the energy barrier in site 3 which constitutes a bottleneck for diffusion of the polaron into the bulk. These results, which show a driving force to bury the extra electron in the lattice when in solution, seem to corroborate a recent study by Williams and Scherer (2004), who observed, with Mössbauer spectroscopy, electron transfer between adsorbed iron(II) and iron(III) from the iron oxide lattice. However, a calculation of the elec-

tron transfer between a Fe(II) adatom and a Fe(III) at the surface would be required for a more direct comparison.

3.3. O(H)-terminated (001) hematite surface

Along the (001) direction, iron bi-layers alternate with close-packed oxygen layers, and thus the (001) surface can be terminated either by a layer of oxygen or iron atoms. As mentioned in the Introduction, both terminations have been observed experimentally and predicted theoretically and hence both were considered in the present study. When generating a stoichiometric (001) surface in vacuum, a slab with a full oxygen layer at the top surface and a full iron bi-layer at the bottom surface is produced. Due to the alternation of planes of opposite charges, there is a net dipole moment perpendicular to the surface. To remove this dipole moment, half of the surface oxygens are translated to the bottom of the slab (Oliver et al., 1993). Hence, the resulting slab has no net dipole moment and is terminated by half a layer of oxygen atoms on each face. An X-ray photoemission study (Liu et al., 1998) showed that a small water vapor pressure ($\sim 10^{-4}$ Torr) was sufficient for the full hydroxylation of the surface to occur. Therefore, our model (001) oxygen-terminated surface consisted of 176 Fe_2O_3 units together with 24 dissociated water molecules to produce a fully hydroxylated, charge-neutral surface on each face of the slab. Fig. 6 shows one half of the model slab. The surface area was 20.29×17.57 Å^2 and the slab thickness was approximately 24 Å using the topmost oxygen layer as the surface plane. Since the direction normal to the surface is the *c* direction, the surface does not break the symmetry of any of the two electron transfers studied so far. Indeed, the basal transfer occurs exclusively within a surface layer and the *c* direction transfer only takes place between two surface layers. This, as we shall see, has important consequences for electron diffusion into the bulk of the mineral. As previously, we allowed the mineral slab to equilibrate in vacuum for 300 ps and we then carried out a series of electron transfer calculations to model the basal and *c* direction transfers in the first four surface layers. The electron transfer parameters thus obtained are summarized in Table 3 and shall now be discussed.

As seen for the (012) surface, there is a clear increase in reorganization energy at the surface (11 and 18% relative to the bulk for the first basal plane and *c* direction transfers, respectively). The reorganization energy then gradually

Table 3
Electron transfer parameters for electron transfer at the (001) hydroxyl-terminated surface both in vacuum and in contact with an aqueous solution

Layer(s)	Transfer	λ (eV)	V_{AB} (eV)	ΔG^0 (eV)	κ	i	ΔG^* (eV)	k (s^{-1})
In vacuum								
1	Basal plane	1.95	0.184	0.08	1.00	3	0.53	9.6E+07
1–2	*c* direction	2.22	0.028	0.01	0.21	1	0.53	2.2E+04
2	Basal plane	1.82	0.184	0.03	1.00	3	0.29	8.4E+08
2–3	*c* direction	2.04	0.028	0.04	0.22	1	0.51	6.1E+04
3	Basal plane	1.75	0.184	−0.07	1.00	3	0.22	1.1E+10
3–4	*c* direction	1.96	0.028	−0.01	0.22	1	0.46	3.9E+05
4	Basal plane	1.73	0.184	−0.01	1.00	3	0.24	5.0E+09
4–5	*c* direction	1.87	0.028	0.00	0.23	1	0.44	7.5E+05
In solution								
1	Basal plane	1.98	0.184	0.16	1.00	3	0.40	1.3E+07
1–2	*c* direction	2.25	0.028	−0.06	0.21	1	0.51	5.8E+04
2	Basal plane	1.90	0.184	0.03	1.00	3	0.31	4.2E+08
2–3	*c* direction	1.96	0.028	0.03	0.22	1	0.48	1.8E+05
3	Basal plane	1.72	0.184	−0.02	1.00	3	0.24	6.0E+09
3–4	*c* direction	1.93	0.028	0.00	0.23	1	0.45	4.4E+05
4	Basal plane	1.75	0.184	0.01	1.00	3	0.26	2.8E+09
4–5	*c* direction	1.90	0.028	−0.01	0.23	1	0.44	6.9E+05

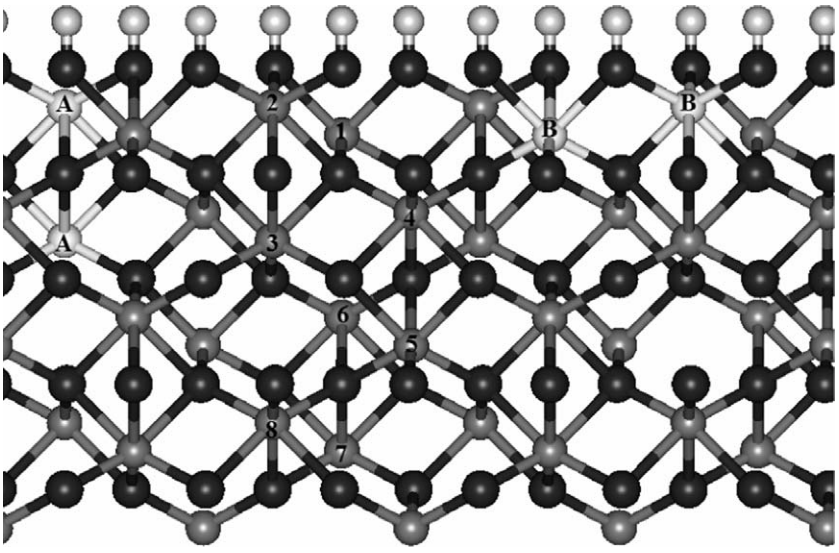

Fig. 6. Side view of the (001) hydroxyl-terminated hematite surface showing the two possible electron transfers, namely *c* direction (A) and basal plane (B). Also shown are the first eight nonequivalent iron sites.

decreases to converge to its bulk value by the third layer for the basal plane transfer and by the fourth layer for the *c* direction transfer. All the electron transfer reactions show small free energies of reaction, often within the accuracy of the method. Fig. 7 shows the free energy profile of a polaron diffusing in the near-surface region generated from the free energies in Table 3. There is only a small overall driving force for the polaron to diffuse to the surface and there is no significant energy barrier for diffusion to and from the bulk. Site 1 is found to be the most energetically favored iron site at this surface although only by 0.07 eV relative to a bulk iron site. Although the free energies of electron transfer are not significantly affected, the adiabatic activation free energies are increased relative to those in the bulk in the first two layers. Again, convergence to bulk values is obtained at the third surface layer.

The mineral slab is then put in contact with an aqueous solution modeled by a water slab containing 355 water molecules. The system is equilibrated for 300 ps and the electron transfer calculations are repeated. Table 3 shows the electron transfer parameters obtained in solution. Water has little effect on the reorganization energy. Also, the relative free energies of different sites are not significantly affected except for site 1 which is stabilized relative to the other sites. The effect of the presence of water on the activation free energy is small except again for the first basal transfer which shows a reduced activation free energy. This confirms what was learned from the previous surface, namely that direct contact between water and the iron site is required to observe a significant water effect.

Due to the presence of the terminal hydroxyl groups, the topmost iron octahedra are complete and thus we would expect the electronic coupling matrix element to be close to that in the bulk. Hence, we used the V_{AB} values obtained from the bulk calculations to compute the rate of all the electron transfers at this surface. In vacuum, the basal transfer at the topmost surface layer shows a decrease in rate of about two orders of magnitude ($9.6 \times 10^7\ s^{-1}$). However, this rate corresponds to an electron transfer from site 1 to site 2 and due to the asymmetry of this electron transfer an electron transfer from site 2 to site 1 is calculated to occur at rate of $1.8 \times 10^9\ s^{-1}$. Therefore, the overall polaron diffusion rate within the first surface layer is a combination of these two rates, both of which are several orders of magnitude higher than the first electron transfer to the second surface layer. Indeed, the rate of the first *c* direction transfer is one order of magnitude lower than in the bulk ($2.2 \times 10^4\ s^{-1}$). This suggests that electron transport at the surface is anisotropic with the in-plane diffusion being about four orders of magnitude faster than the out-of-plane electron transfer. The presence of water does not significantly affect the rates.

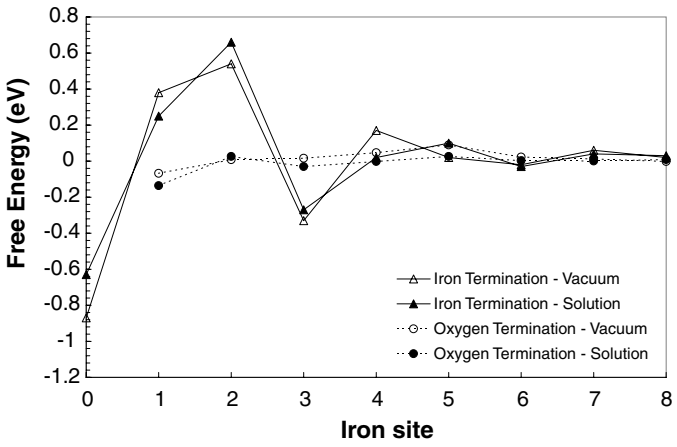

Fig. 7. Free energy profiles of a small polaron diffusing at the (001) hydroxyl- and iron-terminated surfaces in vacuum and in contact with an aqueous solution. The lines are provided as a guide to the eyes.

In summary, as seen with the (012) surface, the reorganization energy and activation free energy increase at the topmost layer, which results in a decrease in rate. But in contrast to the (012) surface, because there is no direct bonding between iron and molecular water, the effect of water is only limited. Finally, due to the orientation of the surface, small polarons can diffuse more readily within a surface layer than between two surface layers and thus the overall electron diffusion into the bulk will be slower than at the (012) surface. This suggests that electrons will reside longer at the surface and thus be able to diffuse over longer lateral distances.

3.4. Fe-terminated (001) hematite surface

The (001) surface can also be cleaved through the cation bi-layer to produce a surface terminated by 1/3 monolayer of iron atoms over the close-packed oxygen layer, as opposed to 2/3 monolayer in the bulk. The model (001) iron-terminated surface used in this study contained 192 Fe_2O_3 units. The surface area and slab thickness are identical to those of the hydroxyl-terminated surface. As was the case at the hydroxyl-terminated surface, the orientation of the surface does not break the symmetry of the two electron transfers. However, we now need to consider an additional direction for electron transfer. Indeed, from the topmost iron atom (labeled 0 in Fig. 8), there is no possible basal or *c* direction electron transfer and electron transfers from this site to sites 1 and 2 will occur between corner-sharing FeO_6 octahedra, as shown by the atoms labeled 'A' in Fig. 8. This particular electron transfer was not considered in the bulk as its rate was expected to be significantly slower than the two electron transfers mentioned so far, for two reasons. First, the two iron atoms are bridged by a single oxygen atom. The importance of bridging oxygen atoms for high electronic coupling has been highlighted previously (Rosso et al., 2003a; Iordanova et al., 2005; Kerisit and Rosso, 2005). Therefore, the electronic coupling is predicted to be weaker than that of the *c* direction transfer, where the two centers are bridged by three oxygen atoms. Second, the electron transfer distance is longer than for the other two electron transfers, 3.63 Å compared to 2.99 and 2.83 Å in the basal and *c* direction transfers, respectively.

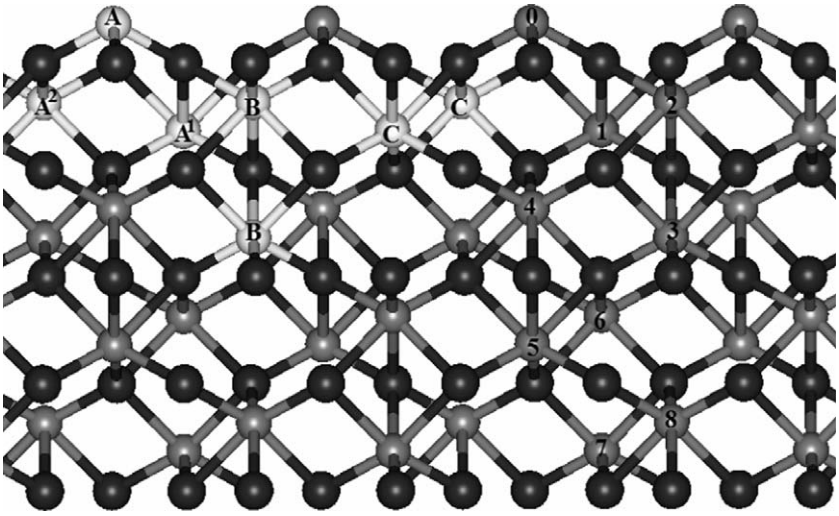

Fig. 8. Side view of the (001) iron-terminated hematite surface showing the three possible electron transfers, namely corner (A), *c* direction (B), and basal plane (C). Note that a corner transfer from site 0 can occur to site 1 or to site 2, shown as A^1 and A^2. Also shown are the first nine nonequivalent iron sites.

Table 4 shows the electron transfer parameters obtained at the iron-terminated surface in vacuum. The reorganization energy for the electron transfers in the first surface layer is reduced by about 0.2 eV compared to the same electron transfers at the hydroxyl-terminated surface. The electron transfers in the second layer are also affected, whereas in the third layer the difference in reorganization energy with the electron transfers at the hydroxyl-terminated surface and in the bulk becomes negligible. Contrary to what was predicted at the hydroxyl-terminated surface, the free energies of reaction are large, mainly in the first two layers. The free energies of electron transfer from site 0 are the largest calculated so far in this study (1.41 and 1.25 eV). A corner transfer from site 0 to site 1 followed by a basal transfer to site 2 is equivalent to a direct electron transfer from site 0 to site 2. It is thus reassuring that our calculations show that the free energy difference between sites 0 and 2 is independent of the path taken. Fig. 7 shows the free energy profile obtained by compiling all the free energy values. The amplitude of the free energy variation as a function of depth is much greater than that calculated at the hydroxyl-terminated surface, although it does also converge by the third layer. Fig. 7 displays a remarkably large free energy barrier for the electron to diffuse in the bulk from site 0. Sites 1 and 2 are particularly energetically unfavorable relative to iron bulk sites. However, these sites are accessible for direct electron transfer from an adsorbed species, which would facilitate injection in the mineral, effectively by-passing the large free energy barrier between site 0 and the bulk. The adiabatic activation free energy also shows large variations as a function of depth. For the first time, we observe a reduction of the activation free energy at the surface in the case of the first *c* direction transfer.

Table 4
Electron transfer parameters for the electron transfer at the (001) iron-terminated surface in both vacuum and in contact with an aqueous solution

Layer(s)	Transfer	λ (eV)	V_{AB} (eV)	ΔG^0 (eV)	κ	i	ΔG^* (eV)	k (s^{-1})
In vacuum								
1	Corner (to 2)	1.40	0.028	1.41	0.41	3	1.38	3.4E−10
1	Corner (to 1)	1.53	0.028	1.25	0.40	3	1.23	1.1E−07
1	Basal plane	1.71	0.184	0.16	1.00	3	0.33	1.8E+08
1–2	*c* direction	2.06	0.028	−0.87	0.36	1	0.14	7.0E+10
2	Basal plane	1.93	0.184	0.50	1.00	3	0.58	1.1E+04
2–3	*c* direction	1.89	0.028	−0.15	0.37	1	0.37	1.0E+07
3	Basal plane	1.70	0.184	−0.04	1.00	3	0.22	1.1E+10
3–4	*c* direction	1.97	0.028	0.08	0.37	1	0.50	6.8E+04
4	Basal plane	1.75	0.184	−0.04	1.00	3	0.23	6.8E+09
4–5	*c* direction	1.96	0.028	−0.02	0.37	1	0.45	4.5E+05
In solution								
1	Corner (to 1)	1.62	0.028	0.88	0.39	3	0.94	9.7E−03
1	Basal plane	1.71	0.184	0.41	1.00	3	0.47	7.0E+05
1–2	*c* direction	2.05	0.028	−0.93	0.36	1	0.12	1.5E+11
2	Basal plane	1.76	0.184	0.29	1.00	3	0.42	5.9E+06
2–3	*c* direction	1.86	0.028	0.08	0.37	1	0.47	1.9E+05
3	Basal plane	1.75	0.184	−0.13	1.00	3	0.19	3.7E+10
3–4	*c* direction	1.92	0.028	0.07	0.37	1	0.49	1.3E+05
4	Basal plane	1.73	0.184	−0.01	1.00	3	0.24	5.0E+09
4–5	*c* direction	1.92	0.028	−0.03	0.37	1	0.44	7.8E+05

The mineral slab is then put in contact with a water slab containing 380 water molecules and is equilibrated for 300 ps. The same electron transfer calculations are repeated except for the corner transfer to site 2 as it is expected to be a great deal slower than that to site 1 and thus should only play a minor role. Again, the effect of water is very similar to what has been observed so far. The reorganization energy is not significantly affected and the free energy of reaction for iron in contact with water is reduced. However, it is worth mentioning that the corner transfer, from site 0 to site 1, shows the largest change in reorganization energy upon hydration of all the topmost layer transfers considered in this work and that the iron atoms at site 0 are exposed to water the most. Hence, the small effect of

hydration could be due to the fact that the electron transfer centers, in each electron transfer considered in the present study, are at most only partially "embedded" in the liquid phase. The reduction in free energy of reaction is not as substantial as at the (012) surface, although the foremost iron atom is coordinated to three water molecules. This could be due to the water–water interactions, which would prevent the water molecules from approaching the iron atoms as close as at the (012) surface and thus each bond would be weaker. Indeed, the iron–water oxygen RDF at the (012) surface shows an average surface iron–water oxygen bond distance of 1.84 Å whereas this value increases to 1.92 Å at the (001) surface.

As mentioned before, the calculation of the electronic coupling for the 'classically spin forbidden' electron transfer is beyond the scope of this paper, hence we used the V_{AB} values obtained from the bulk c direction transfer for the corner transfer. Therefore, this clearly constitutes the upper limit of the possible V_{AB} values for this particular electron transfer. In vacuum, corner electron transfers to sites 1 and 2 are extremely slow when compared to the rates calculated so far (1.1×10^{-7} and $3.4 \times 10^{-10}\ s^{-1}$). This is due to the deep free energy well at this site, as shown in Fig. 7. Although water stabilizes the configuration where an iron(III) is at site 0, which causes the rate to increase by about four orders of magnitude, the rate of electron transfer toward the bulk is still remarkably slow ($9.7 \times 10^{-3}\ s^{-1}$). The calculated rates indicate that the electron is effectively trapped at this site. If dissolution occurs at a higher or similar rate, we would expect the iron atoms in site 0 not to have sufficient time to transfer their 'extra' electron in the lattice and thus to dissolve as iron(II). In addition, the rate of electron transfer in the reversed reaction, namely for an electron in sites 1 and 2 to transfer to site 0, is calculated to be extremely fast (about $10^{14}\ s^{-1}$). This suggests that a polaron diffusing in the surface layer would be rapidly trapped into site 0. These results clearly show that protuberant iron atoms make perfect electron traps and could readily dissolve and increase the concentration of iron(II) in solution. Surface defects that involve undercoordinated iron atoms at the surface could behave similarly.

In summary, the iron-terminated surface shows a surprisingly different behavior than the hydroxyl-terminated surface. Principally, the relative free energies of the iron sites in the first two layers are greatly affected by the surface termination and thus the rates of electron transfer in this region are changed dramatically. This shows that surface features such as defects, kinks, and steps would affect electron transfer properties of the hematite lattice in their vicinity. However, similar characteristics are observed, namely that the electron transfer parameters converge to bulk values from the third surface layer and that water has a limited effect on the reorganization energy. Electron transfers from site 0 do not show a water effect as significant as at the (012) surface. This can be explained by the fact that water cannot approach site 0 as close as it can approach site 1 at the (012) surface.

4. Conclusions

We first carried out molecular dynamics simulations and ab initio calculations to model electron transfer reactions in bulk hematite, whereby the electron transfer occurs by II/III valence interchange between nearest-neighbor iron atoms. Electron transfer parameters and rate constants were in good accord with ab initio electronic structure calculations published previously. Two potential models were evaluated and the Lewis and Catlow model was found to give the closest agreement with Hartree-Fock calculations.

The molecular dynamics method was then successfully applied to the simulation of electron transfer at two low-index hematite surfaces. These calculations show that, in most cases, the reorganization energy increases by 10–25% at the topmost surface layer, which causes the activation free energy to increase and thus the rate of electron transfer in the near-surface region to decrease. It was shown that, in the case of the (012) surface, the increase in reorganization energy is due to the relaxation of the FeO_6 octahedron at the surface. In addition, we repeatedly found that the reorganization energy converges to its bulk value by the third surface layer down.

The large relaxation of the surface octahedra also accounts for the fact that the electronic coupling is diminished at the (012) surface, in both dry and hydrated conditions, hence causing the rate of electron transfer at the surface to decrease further.

The effect of the presence of water in contact with the hematite surfaces was also investigated. Our findings indicate that water has little effect on the reorganization energy. However, it was found that, where there is direct contact between water molecules and iron atoms involved in the electron transfer reaction, water affects the free energy of reaction as well as the activation free energy to a great extent. Water provides a driving force for the polaron to diffuse away from the surface and toward the bulk. The effect is most pronounced when water can adsorb close to the surface, as is the case at the (012) surface. In all the surfaces considered here the influence of water on the electron transfer parameters becomes negligible by the third surface layer.

Our study also shows that there are significant differences between the surfaces considered in this work. Because of the inherent anisotropic conductivity of the hematite lattice, different surfaces will show different rates of electron diffusion in the planes normal and parallel to the surface. Furthermore, results obtained at the (001) surface show that surface termination can also affect the electron transfer properties some distance down into the surface.

Electron transfer simulations at the (001) iron-terminated surface suggest that terminal iron atoms that are strongly undercoordinated can effectively act as electron traps. This implies that surface features such as steps and etch channels can trap electrons thus increasing the local concentration of iron(II) in the lattice which would result in an enhanced dissolution rate at defects. In addition, to

address the question formulated in the Introduction, we have shown that, in the case of the hydroxyl-terminated (001) surface, the in-plane electron transfer rate is three orders of magnitude higher than the inter-layer rate and thus small polarons could cover large lateral distances in the near-surface region before diffusing in the bulk. Although the rate of electron transfer in the first surface layer, in this instance, is lower than in the bulk, it corresponds to a diffusion coefficient of the order of a $\mu m^2\ s^{-1}$ (Rosso et al., 2003a; Iordanova et al., 2005), based on a random walk. These two facts may explain the observations made by Rosso et al. (2003b), who utilized hematite platelets that were 20 μm across and exposed the basal plane. However, further work is required to investigate electron diffusion over longer time and length scales and to incorporate other important factors, such as polaron–polaron interactions, in order to construct the next generation model. Therefore, in the future, we will use the rates of electron transfer calculated in this work to study the diffusion of electrons injected in the hematite lattice in a Kinetic Monte Carlo simulation.

Acknowledgments

The authors are grateful for the comments of Jim Rustad, Woods Halley, and two anonymous reviewers for improving the manuscript. The authors wish to acknowledge support for this work from the Pacific Northwest National Laboratory under the Biogeochemistry Grand Challenge Project. We also gratefully acknowledge the support of the Stanford Environmental Molecular Sciences Institute (EMSI) jointly funded by the National Science Foundation (NSF) and the US Department of Energy's (DOE) Office of Biological and Environmental Research (OBER). This research was performed in part using the Molecular Science Computing Facility (MSCF) in the William R. Wiley Environmental Molecular Sciences Laboratory, a national scientific user facility sponsored by the US Department of Energy's Office of Biological and Environmental Research and located at the Pacific Northwest National Laboratory. Pacific Northwest is operated for the Department of Energy by Battelle.

Associate editor: James Rustad

Appendix A. Supplementary data

Supplementary data associated with this article can be found, in the online version, at doi:10.1016/j.gca.2005.12.021.

References

Ayub, I., Berry, F.J., Bilsborrow, R.L., Helgason, O., Mercader, R.C., Moore, E.A., Stewart, S.J., Wynn, P.G., 2001. Influence of zinc doping on the structural and magnetic properties of α-Fe_2O_3. *J. Solid State Chem.* **156**, 408–414.

Baram, P.S., Parker, S.C., 1996. Atomistic simulation of hydroxide ions in inorganic solids. *Philos. Mag. B* **73**, 49–58.

Benjelloun, D., Bonnet, J.P., Doumerc, J.P., Launey, J.C., Onillon, M., Hagenmuller, P., 1984. Anisotropy of the electrical-properties of iron-oxide α-Fe_2O_3. *Mater. Chem. Phys.* **10**, 503–518.

Berry, F.J., Bohorquez, A., Greaves, C., McManus, J., Moore, E.A., Mortimer, M., 1998. Structural characterization of divalent magnesium-doped α-Fe_2O_3. *J. Solid State Chem.* **140**, 428–430.

Berry, F.J., Bohorquez, A., Moore, E.A., 1999. Rationalisation of defect structure of tin- and titanium-doped α-Fe_2O_3 using interatomic potential calculations. *Solid State Commun.* **109**, 207–211.

Born, M., Huang, K., 1954. *Dynamical Theory of Crystal Lattices*. Oxford University Press, Oxford, UK.

Bush, T.S., Gale, J.D., Catlow, C.R.A., Battle, P.D., 1994a. Self-consistent interatomic potentials for the simulation of binary and ternary oxides. *J. Mater. Chem.* **4**, 831–837.

Bush, T.S., Gale, J.D., Catlow, C.R.A., Battle, P.D., 1994b. Self-consistent interatomic potentials for the simulation of binary and ternary oxides (corrigenda). *J. Mater. Chem.* **4**, 1765.

Chambers, S.A., Yi, S.I., 1999. Fe termination for α-Fe_2O_3 (001) as grown by oxygen-plasma-assisted molecular beam epitaxy. *Surf. Sci.* **439**, L785–L791.

Clark, T., Chandrasekhar, J., Spitznagel, G.W., Schleyer, P.V., 1983. Efficient diffuse function-augmented basis-sets for anion calculations.3. The 3-21+G basis set for 1st-row elements, Li-F. *J. Comput. Chem.* **4**, 294–301.

Condon, N.J., Leibsle, F.M., Lennie, A.R., Murray, P.W., Parker, T.M., Vaughan, D.J., Thornton, G., 1998. Scanning tunnelling microscopy studies of α-Fe_2O_3 (0001). *Surf. Sci.* **397**, 278–287.

Cooke, D.J., Redfern, S.E., Parker, S.C., 2004. Atomistic simulation of the structure and segregation to the (00.1) and (01.2) surfaces of Fe_2O_3. *Phys. Chem. Minerals* **31**, 1–11.

Curtiss, L.A., Halley, J.W., Hautman, J., Rahman, A., 1987. Nonadditivity of ab initio pair potentials for molecular dynamics of multivalent transition metal in water. *J. Chem. Phys.* **86**, 2319–2327.

Davies, M.J., Kenway, P.R., Lawrence, P.J., Parker, S.C., Mackrodt, W.C., Tasker, P.W., 1989. Impurity segregation to the surfaces of corundum-structured oxides. *J. Chem. Soc., Faraday Trans.* **85**, 555–563.

de Leeuw, N.H., Parker, S.C., 1998. Molecular-dynamics simulation of MgO surfaces in liquid water using a shell-model potential for water. *Phys. Rev. B* **58**, 13901–13908.

Dick, B.G., Overhauser, A.W., 1958. Theory of the dielectric constants of alkali halide crystals. *Phys. Rev.* **112**, 90–103.

Eggleston, C.M., Stack, A.G., Rosso, K.M., Higgins, S.R., Bice, A.M., Boese, S.W., Pribyl, R.D., Nichols, J.J., 2003. The structure of hematite (α-Fe_2O_3) (001) surfaces in aqueous media: scanning tunneling microscopy and resonant tunneling calculations of coexisting O and Fe terminations. *Geochim. Cosmochim. Acta* **67**, 985–1000.

Ewald, P.P., 1921. Die Berechnung optischer und elektrostatischer Gitterpotentiale. *Ann. Phys.* **64**, 253–287.

Farazdel, A., Dupuis, M., Clementi, E., Aviram, A., 1990. Electric field induced intramolecular electron transfer in spiro π-electron systems and their suitability as molecular electronic devices. A theoretical study. *J. Am. Chem. Soc.* **112**, 4206–4214.

Gharibi, E., Hbika, A., Dupre, B., Gleitzer, C., 1990. Electrical properties of pure and titanium-doped hematite single crystals, in the basal plane, at low oxygen pressure. *Eur. J. Solid State Inorg. Chem.* **27**, 647–658.

Goodenough, J.B., 1971. In: Heiss, H. (Ed.), *Progress in Solid State Chemistry*, vol. 5. Pergamon, NY, pp. 298–301.

Henderson, M.A., 2002. Insights into the (1×1)-to-(2×1) phase transition of the α-Fe_2O_3 (012) surface using EELS, LEED and water TPD. *Surf. Sci.* **512**, 253–262.

Henderson, M.A., 2003. Surface stabilization of organics on hematite by conversion from terminal to bridging adsorption structures. *Geochim. Cosmochim. Acta* **67**, 1055–1063.

Henderson, M.A., Joyce, S.A., Rustad, J.R., 1998. Interaction of water with the (1×1) and (2×1) surfaces of α-Fe_2O_3 (012). *Surf. Sci.* **417**, 66–81.

Holstein, T., 1959a. Studies of polaron motion I. The molecular-crystal model. *Ann. Phys.* **8**, 325–342.

Holstein, T., 1959b. Studies of polaron motion II. The 'small' polaron. *Ann. Phys.* **8**, 343–389.

Hoover, W.G., 1985. Canonical dynamics – equilibrium phase-space distributions. *Phys. Rev. A* **31**, 1695–1697.

Hwang, J.K., Warshel, A., 1987. Microscopic examination of free-energy relationships for electron-transfer in polar-solvents. *J. Am. Chem. Soc.* **109**, 715–720.

Iordanova, N., Dupuis, M., Rosso, K.M., 2005. Charge transport in metal oxides: a theoretical study of hematite α-Fe_2O_3. *J. Chem. Phys.* **122**, 144305.

Jones, F., Rohl, A.L., Barrow, J.B., van Bronswijk, W., 2000. Molecular modeling of water adsorption on hematite. *Phys. Chem. Chem. Phys.* **2**, 3209–3216.

Junta-Rosso, J.L., Hochella Jr., M.F., 1996. The chemistry of hematite {001} surfaces. *Geochim. Cosmochim. Acta* **60**, 305–314.

Kerisit, S., Cooke, D.J., Spagnoli, D., Parker, S.C., 2005. Molecular dynamics simulations of the interaction between water and inorganic solids. *J. Mater. Chem.* **15**, 1454–1462.

Kerisit, S., Parker, S.C., 2004. Free energy of adsorption of water and metal ions on the {10.4} calcite surface. *J. Am. Chem. Soc.* **126**, 10152–10161.

Kerisit, S., Rosso, K.M., 2005. Charge transfer in FeO: a combined molecular-dynamics and ab initio study. *J. Chem. Phys.* **123**, 224712.

King, G., Warshel, A., 1990. Investigation of the free-energy functions for electron-transfer reactions. *J. Chem. Phys.* **93**, 8682–8692.

Krishnan, R., Binkley, J.S., Seeger, R., Pople, J.A., 1980. Self-consistent molecular orbitals. XX. A basis set for correlated wave functions. *J. Chem. Phys.* **72**, 650–654.

Kuharski, R.A., Bader, J.S., Chandler, D., Sprik, M., Klein, M.L., Impey, R.W., 1988. Molecular-model for aqueous ferrous ferric electron-transfer. *J. Chem. Phys.* **89**, 3248–3257.

Lewis, G.V., Catlow, C.R.A., 1985. Potential models for ionic oxides. *J. Phys. C: Solid State Phys.* **18**, 1149–1161.

Liu, P., Kendelewicz, T., Brown Jr., G.E., Nelson, E.J., Chambers, S.A., 1998. Reaction of water vapor with α-Al_2O_3 (0001) and α-Fe_2O_3 (0001) surfaces: synchrotron X-ray photoemission studies and thermodynamic calculations. *Surf. Sci.* **417**, 56–65.

Lovley, D.R., 1991. Dissimilatory Fe(III) and Mn(IV) reduction. *Microbiol. Rev.* **55**, 259–287.

Lovley, D.R., Coates, J.D., Blunt-Harris, E.L., Phillips, E.J.P., Woodward, J.C., 1996. Humic substances as electron acceptors for microbial respiration. *Nature* **382**, 445–448.

Marcus, R.A., Sutin, N., 1985. Electron transfers in chemistry and biology. *Biochim. Biophys. Acta* **811**, 265–322.

Melchionna, S., Ciccotti, G., Holian, B.L., 1993. Hoover NPT dynamics for systems varying in shape and size. *Mol. Phys.* **78**, 533–544.

Mitchell, P.J., Fincham, D., 1993. Shell model simulations by adiabatic dynamics. *J. Phys.: Condens. Matter* **5**, 1031–1038.

Moore, E.A., Widatallah, H.M., Berry, F.J., 2002. Prediction of defect structure in lithiated tin- and titanium-doped α-Fe_2O_3 using atomistic simulation. *J. Phys. Chem. Solids* **63**, 519–523.

Nakau, T., 1960. Electrical conductivity of α-Fe_2O_3. *J. Phys. Soc. Jpn.* **15**, 727.

Neal, A.L., Rosso, K.M., Geesey, G.G., Gorby, Y.A., Little, B.J., 2003. Surface structure effects on direct reduction of iron oxides by Shewanella oneidensis. *Geochim. Cosmochim. Acta* **67**, 4489–4503.

Nelsen, S.F., Blackstock, S.C., Kim, Y., 1987. Estimation of inner shell Marcus terms for amino nitrogen-compounds by molecular-orbital calculations. *J. Am. Chem. Soc.* **109**, 677–682.

Newman, D.K., Kolter, R., 2000. A role for excreted quinones in extracellular electron transfer. *Nature* **405**, 94–97.

Oliver, P.M., Parker, S.C., Mackrodt, W.C., 1993. Computer-simulation of the crystal morphology of NiO. *Model. Simul. Mater. Sci. Eng.* **1**, 755–760.

Papaioannou, J.C., Patermarakis, G.S., Karayianni, H.S., 2005. Electron hopping mechanism in hematite (α-Fe_2O_3). *J. Phys. Chem. Solids* **66**, 839–844.

Parker, S.C., de Leeuw, N.H., Redfern, S.E., 1999. Atomistic simulation of oxide surfaces and their reactivity with water. *J. Chem. Soc., Faraday Discussions* **114**, 381–393.

Rohrbach, A., Hafner, J., Kresse, G., 2004. Ab initio study of the (0001) surfaces of hematite and chromia: Influence of strong electronic correlations. *Phys. Rev. B* **70**, 125426.

Rosso, K.M., Dupuis, M., 2004. Reorganization energy associated with small polaron mobility in iron oxide. *J. Chem. Phys.* **120**, 7050–7054.

Rosso, K.M., Smith, D.M.A., Dupuis, M., 2003a. An ab initio model of electron transport in hematite (α-Fe_2O_3) basal planes. *J. Chem. Phys.* **118**, 6455–6466.

Rosso, K.M., Zachara, J.M., Fredrickson, J.K., Gorby, Y.A., Smith, S.C., 2003b. Nonlocal bacterial electron transfer to hematite surfaces. *Geochim. Cosmochim. Acta* **67**, 1081–1087.

Rustad, J.R., Rosso, K.M., Felmy, A.R., 2004. Molecular dynamics investigation of ferrous-ferric electron transfer in a hydrolyzing aqueous solution: Calculation of the pH dependence of the diabatic transfer barrier and the potential of mean force. *J. Chem. Phys.* **120**, 7607–7615.

Rustad, J.R., Wasserman, E., Felmy, A.R., 1999. Molecular modeling of the surface charging of hematite II. Optimal proton distribution and simulation of surface charge versus pH relationships. *Surf. Sci.* **424**, 28–35.

Schafer, A., Huber, C., Ahlrichs, R., 1994. Fully optimized contracted gaussian-basis sets of triple zeta valence quality for atoms Li to Kr. *J. Chem. Phys.* **100**, 5829–5835.

Shaikhutdinov, S.K., Weiss, W., 1999. Oxygen pressure dependence of the α-Fe_2O_3 (0001) surface structure. *Surf. Sci.* **432**, L627–L634.

Shapira, Y., 1969. Ultrasonic behavior near the spin-flop transitions of hematite. *Phys. Rev.* **184**, 560–589.

Smith, W., Forester, T.R., 1996. DL_POLY is a package of molecular simulation routines, copyright The Council for the Central Laboratory of the Research Councils, Daresbury Laboratory at Daresbury, Nr. Warrington.

Straatsma, T.P., Apra, E., Windus, T.L., Dupuis, M., Bylaska, E.J., de Jong, W., Hirata, S., Smith, D.M.A., Hackler, M.T., Pollack, L., Harrison, R.J., Nieplocha, J., Tipparaju, V., Krishnan, M., Auer, A.A., Brown, E., Cisneros, G., Fann, G., Fruchtl, H., Garza, J., Hirao, K., Kendall, R., Nichols, J.A., Tsemekhman, K., Valiev, M., Wolinski, K., Anchell, J., Bernholdt, D., Borowski, P., Clark, T., Clerc, D., Dachsel, H., Deegan, M., Dyall, K., Elwood, D., Glendening, E., Gutowski, M., Hess, A., Jaffe, J., Johnson, B., Ju, J., Kobayashi, R., Kutteh, R., Lin, Z., Littlefield, R., Long, X., Meng, B., Nakajima, T., Niu, S., Rosing, M., Sandrone, G., Stave, M., Taylor, H., Thomas, G., van Lenthe, J., Wong, A., Zhang, Z., 2004. NWChem, A Computational Chemistry Package for Parallel Computers, Version 4.6, Pacific Northwest National Laboratory, Richland, Washington 99352-0999, USA.

Thevuthasan, S., Kim, Y.J., Yi, S.I., Chambers, S.A., Morais, J., Denecke, R., Fadley, C.S., Liu, P., Kendelewicz, T., Brown Jr., G.E., 1999. Surface structure of MBE-grown α-Fe_2O_3 (0001) by intermediate-energy X-ray photoelectron diffraction. *Surf. Sci.* **425**, 276–286.

Trainor, T.P., Chaka, A.M., Eng, P.J., Newville, M., Waychunas, G.A., Catalano, J.G., Brown Jr., G.E., 2004. Structure and reactivity of the hydrated (001) hematite surface. *Surf. Sci.* **573**, 204–224.

Wang, X.G., Weiss, W., Shaikhutdinov, S.K., Ritter, M., Petersen, M., Wagner, F., Schlögl, R., Scheffler, M., 1998. The hematite (α-Fe_2O_3) (0001) surface: evidence for domains of distinct chemistry. *Phys. Rev. Lett.* **81**, 1038–1041.

Wasserman, E., Rustad, J.R., Felmy, A.R., 1999. Molecular modeling of the surface charging of hematite I. The calculation of proton affinities and acidities on a surface. *Surf. Sci.* **424**, 19–27.

Wasserman, E., Rustad, J.R., Felmy, A.R., Hay, B.P., Halley, J.W., 1997. Ewald methods for polarizable surfaces with application to hydroxylation and hydrogen bonding on the (012) and (001) surfaces of α-Fe_2O_3. *Surf. Sci.*, 385.

Williams, A.G.B., Scherer, M.M., 2004. Spectroscopic evidence for Fe(II)-Fe(III) electron transfer at the iron oxide water interface. *Environ. Sci. Technol.* **38**, 4782–4790.

Woodley, S.M., Battle, P.D., Gale, J.D., Catlow, C.R.A., 1999. The prediction of inorganic crystal structures using a genetic algorithm and energy minimisation. *Phys. Chem. Chem. Phys.* **1**, 2535–2542.

Yamashita, J., Kurosawa, T., 1958. On electronic current in NiO. *J. Phys. Chem. Solids* **5**, 34–43.

Zachara, J.M., Fredrickson, J.K., Li, S.M., Kennedy, D.W., Smith, S.C., Gassman, P.L., 1998. Bacterial reduction of crystalline Fe^{3+} oxides in single phase suspensions and subsurface materials. *Am. Miner.* **83**, 1426–1443.